

# Vision-Based Self-Adaptive Gripping in a Trimodal Robotic Sorting End-Effector

Rasoul Sadeghian, Shahrooz Shahin, Sina Sareh, *Member, IEEE*

**Abstract**— Recyclable waste management, which includes sorting as a key process, is a crucial component of maintaining a sustainable ecosystem. The use of robots in sorting could significantly facilitate the production of secondary raw materials from waste in the sense of a recycling economy. However, due to the complex and heterogeneous types of the recyclable items, the conventional robotic gripping end-effectors, which typically come with a fixed structure, are unlikely to hold onto the full range of items to enable separation and recycling. To this end, a trimodal adaptive end-effector is proposed that can be integrated with robotic manipulators to improve their gripping versatility. The end-effector can deploy effective modes of gripping to different objects in response to their size and porosity via gripping mechanisms based on Nano Polyurethane (PU) adhesive gels, pumpless vacuum suction, and radially deployable claws. While the end-effector’s mechanical design allows the three gripping modes to be deployed independently or in conjunction with one another, this work aims at deploying modes that are effective for gripping onto the recyclable item. In order to decide on the suitable modes of gripping, a real-time vision system is designed to measure the size and porosity of the recyclable items and advise on a suitable combination of gripping modes to be deployed. Integrated current sensors provide an indication of successful gripping and releasing of the recyclable items. The results of the experiments confirmed the ability of our vision-based approach in identifying suitable gripping modes in real-time, the deployment of the relevant mechanisms and successful gripping onto a maximum of 84.8% (single-mode), 90.9% (dual-mode) and 96.9% (triple-mode) of a specified set of recyclable items.

## I. INTRODUCTION

While the culture of consumerism is continuing to increase waste generation, efficient recycling can contribute to a more sustainable environment for us and future generations. The first step in recycling of the waste is separating them into different elements, a process called sorting.

Industrial robotic manipulators can enable a much faster and safer sorting of recyclable items. They are integrated with a range of sensors, such as computer vision, enabling them to monitor the waste stream and use appropriate artificial

intelligence algorithms to identify the waste items, and then the robotic manipulator gets hold of them [1].

Prominent examples include the Heavy Picker (ZenRobotics, Helsinki, Finland) and SELMA (OP Teknik AB, Sweden) that use two-finger heavy duty robotic grippers and arms, and artificial intelligence, to sort construction and demolition waste.

In MAX-AI AQc (Bulk Handling Systems, Oregon, USA) and Machinex SamurAI (Machinex Industries, QC, Canada), Deep Learning is used to identify objects, and an arm with suction cups is mounted above the conveyor belt which moves the identified objects from their position into lateral outlets.

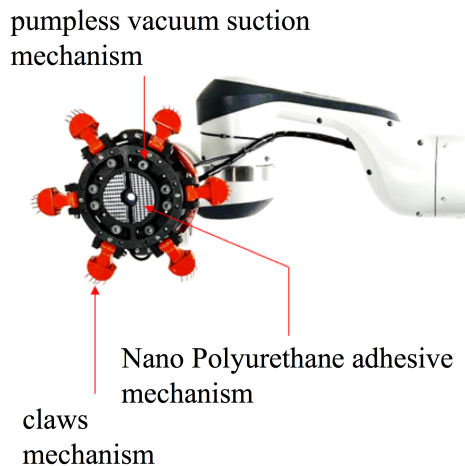


Fig. 1. Adaptive vision-based trimodal sorting end-effector that can autonomously deploy a suitable combination of gripping mechanisms via Nano Polyurethane adhesive gels, pumpless vacuum suction, and claws, based on the surface structure and size of the recyclable item.

However, these systems suffer from a number of key limitations related to the complex and heterogeneous types of recyclable items that are often also combined with surface contamination. The items coming with different sizes, shapes and surface structure cannot be handled using a gripper mechanism with fixed structure, e.g., based on suction cups or multi-finger grasping tools. In addition, the contamination

Manuscript received: September, 09, 2021; Revised November, 28, 2021; Accepted December, 21, 2021. This paper was recommended for publication by Editor Youngjin Choi upon evaluation of the Associate Editor and Reviewers’ comments. This work is supported by the EPSRC UKRI Fellowship (EP/S001840/1).

R. Sadeghian, S. Shahin, and S. Sareh are with RCA Robotics Laboratory, Royal College of Art, London, UK. (email:{rasoul.sadeghian, shahrooz.shahin, sina.sareh}@rca.ac.uk). (Corresponding author: sina.sareh@rca.ac.uk).

makes them hard to recognize via deep learning algorithms that rely on restricted datasets.

In order for a robotic manipulator to successfully handle this job, it should be integrated with a versatile and adaptable gripping mechanism that can enable attachment to a variety of surface structures, shapes and sizes of the recyclable waste items.

Innovative multi-modal gripping systems could be adopted to provide a solution to the gripping versatility issues. Learning from nature, a number of researchers have developed dual-mode grippers using vacuum suction cups and parallel jaws where only one mode of gripping can be activated at a time [2-4], and the two modes can be activated simultaneously to reinforce one another's effect [5]. However, the above dual-mode grippers are unable to hold objects such as porous objects larger than the opening of the gripper.

Modes of attachment such as spines, hooks, and claws are uncommon in gripping systems used for object manipulation, as their sharp edges can damage the objects, while they are popular for use in robotic anchoring mechanisms to porous surfaces [6-8]. However, in the case of a gripper for sorting recyclable waste items, the use of a claw mechanism can be very beneficial enabling gripping onto a wider range of objects, while potential damages to waste items are not concerning.

As such robotic systems should operate over long durations of time to sort large volumes of recyclable items, energy efficiency is an important design parameter. Hence, while the combinational activation of different modes of gripping can be beneficial, a gripping mode should be activated only if it is expected to be effective for gripping onto a specified recyclable item. For example, vacuum suction should not be deployed for gripping onto an object with a porous surface, as this approach is ineffective and wasteful in terms of energy management [6].

Deciding on suitable modes of gripping is another challenge in multi-modal grippers that depend on the features of the recyclable item. Many recent studies on object detection and feature extraction used for gripping have relied on deep learning algorithms. Faster RCNN [8], Mask RCNN [9], YoloV3 [10], and SSD [11] are some of the relatively fast-response deep learning algorithms used for this purpose.

While the use of deep learning approaches has demonstrated some advantages in object detection, including in sorting processes [12], the cross-contamination between recyclable waste items can confuse the detection process. In addition, using very large databases has significant negative impacts on the processing speed and makes the process slower. Therefore, the use of fast vision-based approaches that are not based on deep learning is considered in this study.

The contributions of this paper include creating a trimodal gripping system for waste sorting integrating three mechanisms based on Nano Polyurethane adhesive gels, pumpless vacuum suction, and radially deployable claws that can be independently activated. In order to decide on the suitable modes of gripping, a real-time vision system, based on an improved contour detection algorithm, is designed to measure the recyclable item's features and advise on a

suitable combination of gripping modes to be deployed. Our approach works based on detecting the size and porosity of the recyclable item instead of identifying the item, which makes the decision-making process faster.

The remainder of this paper is organized as follows. In Section II, our approach to the development of the trimodal gripping hardware is described. In Section III, the autonomous vision-based decision-making algorithm developed in this study is explained. The experimental testing of the gripping system and respective results constitute Section IV. The conclusions and future works are presented in Section V.

## II. TRIMODAL GRIPPING END-EFFECTOR MODULE HARDWARE

The claws, Nano PU adhesive, and vacuum suction mechanisms are combined into a trimodal gripping module, Fig. 1. The claws mechanism is used to grip onto the porous surfaces or act as sharp fingertips to hold the recyclable items by using their edges, the vacuum suction mechanism is used to attach to non-porous and smooth surfaces, and the Nano PU adhesive mechanism is used to attach to smooth porous or non-porous surfaces. Each gripping mechanism can work independently, but they can also reinforce each other in gripping and holding the object, if necessary.

In our experimental setup, the payload of the trimodal gripping module is restricted by the payload of the Franka Emika Panda robotic manipulator on which the gripping module is installed. The robotic manipulator has a payload of 3 kg from which 0.84 kg is occupied by the weight of the gripping module. Therefore, the maximum weight of each recyclable item cannot exceed 2.16 kg to satisfy the manipulator's payload limits.

### A. Claws Mechanism

The claws mechanism, which is made via modifying standard fishing hooks, enables not only gripping onto porous objects, as reported in our previous work [6][8], but also acting as sharp fingertips to hold thin non-porous objects (recyclable items) from their edges, when the claws are arranged around the periphery of the recyclable item, Fig. 2a. This mode can particularly reinforce the other two modes when they are used in combination.

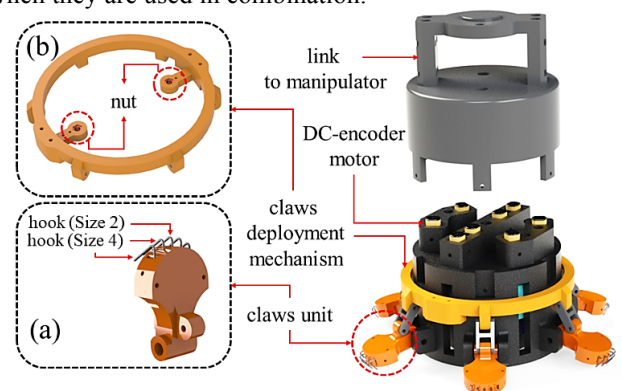


Fig. 2. The claws mechanism: (a) the structure of a claw unit integrating five modified fishing hooks, (b) the motion of claw units are coupled with a sliding ring actuated by two DC encoder motors.

Six claw units are used in our trimodal end-effector, as shown in Fig. 2, with five modified fishing hooks integrated into each of them. Note that fishing hooks are originally designed to be bent, making them difficult to remove once engaged. As a result, we modified them to make detachment easier [6]. The motion of all claw units is coupled with a sliding ring which is actuated via two DC encoder motors running at 500 rounds per minute (rpm), Fig. 2b. The claw units, sliding ring, and linkages are fabricated using Onyx™ materials via a Mark 2 3D printing machine, Markforged, USA.

### B. Pumpless Vacuum Suction Mechanism

The vacuum suction gripping mechanism [13] consists of eight vacuum suction cups (ESS-10-BS, Festo Ltd., Germany) and a custom valve mechanism built within the cup. Each of the four vacuum suction cups is integrated within a hollow semicircular housing filled with super-soft silicone rubber (Mold Max™ 14NV, Smooth-On, USA), as shown in Fig. 3a. DC-encoder motors are used to move the housings that the suction cups are installed on. Each housing is paired with a push-plate that integrates six valve plugs. The valve plugs are used to block and seal the suction cup inlet when the cup is compressed.

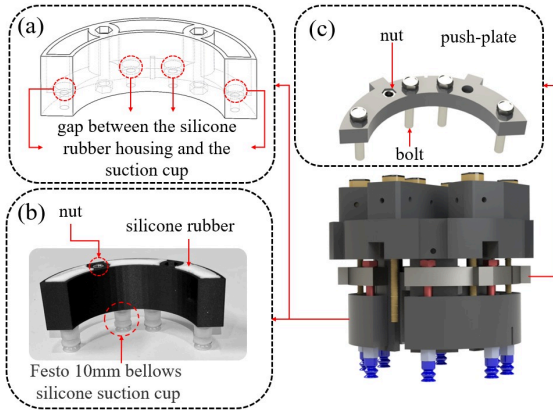


Fig. 3. Pumpless vacuum suction: (a) the semicircular housing integrating four suction cups, (b) the housing is filled with Mold Max™ 14NV silicone rubber materials, (c) the push-plate integrating suction cup inlet plugs. Note that by filling the hollow structure of the housing with silicone materials and allowing a 1mm gap between the cup's inlet and the plug, a faster sealing is achieved.

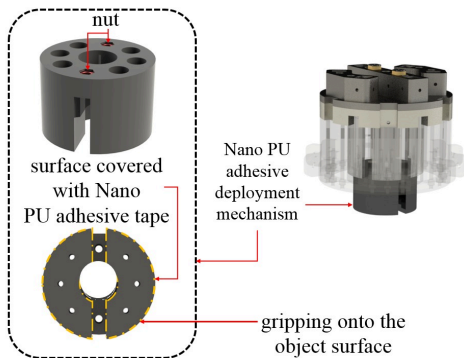
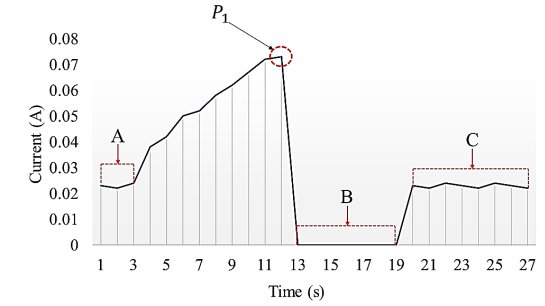


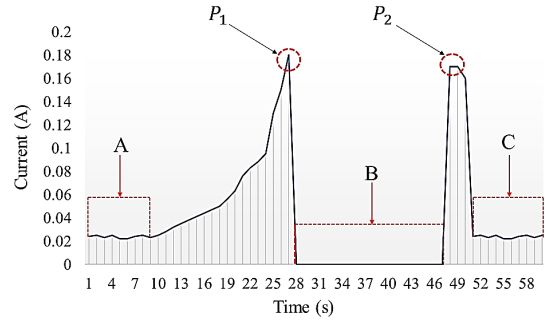
Fig. 4. The structure of the Nano PU adhesive gel mechanism. Note that releasing is enabled by moving the adhesive away from the item's surface into a confined space inside the end-effector.

### C. Nano PU Adhesive Mechanism

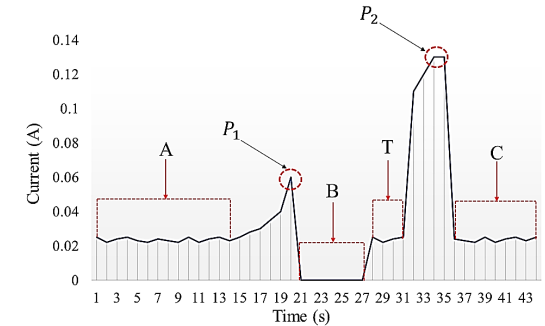
Nano PU adhesive gels is used as an adhesive mechanism, as described in Fig. 4. Two encoder motors are utilized to press the adhesive against the surface of the recyclable item to enable attachment. To release the item, the same set of motors move the adhesive away from the item's surface into a confined space inside the end-effector where the item cannot enter, as described in Fig. 4.



(a) Vacuum suction mechanism.



(b) Claws mechanism.



(c) Nano PU adhesive mechanism.

Fig 5. The current consumption profile of end-effector motors during gripping via different mechanisms.

### D. The module's electronics and processing unit

The module's electronics and processing unit is responsible for processing images from the contact surface, making decisions about suitable modes of gripping to deploy, and providing relevant control signals for motor drivers. The main control board used in this study is NVIDIA® Jetson Xavier NX™, while the motor driver and encoders are controlled by an Arduino Uno. The processing unit is linked to an endoscopic camera that provides visual information from the contact surface. The object size and porosity determination and autonomous decision-making algorithms are run on the main control board, which sends commands to the interface board for the deployment of appropriate gripping modes.

The three gripping mechanisms are deployed using DC encoder motors, with the relevant motor encoder signals being fed back to the Arduino Uno to stop the motors after each mechanism is fully deployed. Furthermore, the feedback from the motors' encoders is used to determine the gripping end-effector's displacement. Also the feedback from current sensors (ACS712) is used to determine whether a gripping mode is fully deployed or not. Fig. 5 shows the output of the current sensors connected to each of the encoder motors in use.

In Fig. 5, A, C indicate the changes in current during no-load deployment of each mechanism before gripping and after releasing the recyclable item. This value is measured to be between 0.019 A to 0.25 A. After gripping onto the item the motors are turned off and this state is indicated as B where the measured current is zero, Fig. 5.

The parameter T in Fig. 5c presents the changes of current before the recyclable item, which is gripped by Nano PU adhesive mechanism, collides with the end-effector's body; after the collision, the current will be increased until the recyclable item is released from the gripping mechanism. Moreover,  $P_1$  and  $P_2$  are the maximum current when the gripping mechanism holds the item and begins to release it, respectively, Fig. 5b and 5c. In the case of the pumpless vacuum suction mechanism,  $P_2$  does not exist since during the releasing process there is no external load applied from the item on the gripping mechanism, Fig. 5a. According to our test results, the maximum measured values of  $P_1$  are 0.061 A (Nano PU adhesive), 0.073 A (vacuum suction), and 0.186 A (claws) mechanisms. These values are used to send a stop command to the system and mark the end of the gripping operation.

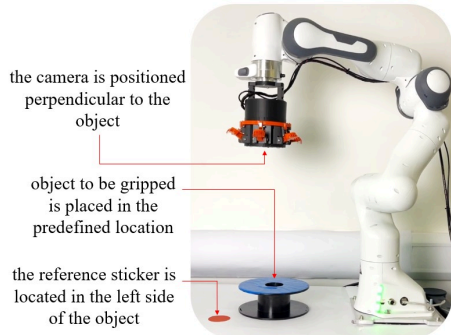


Fig. 6. The configuration of the experimental setup for vision-based decision making on suitable modes of gripping to a specific recyclable item.

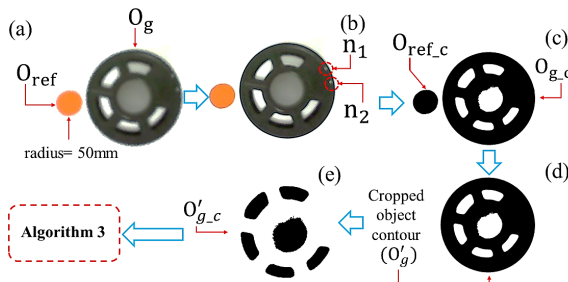


Fig. 7. The outputs of Algorithms 1 (contour detection and scaling) and Algorithm 2 (hole detection and scaling) are fed to Algorithm 3 to decide on suitable modes of gripping.

### III. VISION-BASED AUTONOMOUS DECISION-MAKING

The key stages in the implementation of our vision-based detection system to identify features of the recyclable items are as follows: (1) detecting the reference object ( $O_{ref}$ ), (2) calculating the pixel size of the reference object in millimeters, (3) detecting the object to be gripped  $O_g$ , (4) calculating the size of  $O_g$ , (5) extracting the features of  $O_g$  (size and porosity), and (6) selecting the appropriate gripping mode based on the extracted size and porosity of the items.

#### A. Object Detection and Size Determination

As the reference object, a circular orange sticker is placed on the left side of the predefined grasping point. The diameter of the  $O_{ref}$  is 50 mm. It is easy to distinguish  $O_{ref}$  from  $O_g$ s based on its color and location. Fig. 6 shows the position of the reference object on the robot workspace, as well as the position of the integrated endoscopic camera. The camera is able to capture 30 frames in a single second of video with a 70-degree viewing angle, and a resolution of 1280×720 pixels.

The process of detecting  $O_{ref}$  and calculating its pixel size is described in Algorithm 1. The main two packages used in this algorithm are Numpy and OpenCV(cv2). The radius of  $O_{ref}$  is initialized in the first step, line1, Algorithm 1, Fig. 7a. Then, a Gaussian filter is used to smoothen and remove blur from the relevant camera frame ( $f_i$ ), [14]. The RGB frame is converted to grayscale to remove unnecessary data, resulting in a shorter processing time [15]. Moreover, OpenCV's cv2.erode and cv2.dilate [16] functions are used to connect the broken parts of the detected areas, line4, Algorithm 1, Fig. 7b. The parameter  $f_{i_r}$  in Algorithm 1 is defined as the refined input image. Subsequently, the object's contours ( $O_A$ ), were detected using OpenCV's findContours function, line 5, Algorithm 1. Note that  $O_{ref}$  and  $O_g$  are the items that will be detected at this step, Fig. 7c; if the detected contours' area are less than the predefined minimum value, it will be considered as noise and eliminated, line 6-10, Algorithm 1. The  $n_1$  and  $n_2$  in Fig. 7b present the area that have been neglected in the process of contour detection, Fig. 7c.

The detected contours were then sorted from left to right using OpenCV's contour sorting function (contours.sort contours). The parameters  $O_{ref,c}$ ,  $O_{g,c}$  are presented as the detected  $O_{ref}$  and  $O_g$  contours, Fig. 7c. As a result,  $O_{ref}$  will always be the first item discovered, followed by  $O_g$ . Then the OpenCV's contourArea function is used to calculate the area of the detected object's contour and the number of non-zero pixels. The minAreaRect function in OpenCV is used to calculate the smallest bounding rectangle that can cover the detected contour. The BoxPoints function of OpenCV is employed to determine the rotating bounding box, line 11, Algorithm 1.

Finally, by using the pixels\_per\_metric [17] method the actual size of the object will be determined. The parameters  $O_{ref,c}^{nP}$ ,  $O_{g,c,box}^{nP}$ ,  $O_{ref,c,box}^{nP}$ , and  $O_{g,c,box}^{nP}$  are non-zero detected pixels of  $O_{ref}$  and  $O_g$ s', and the minimum rectangular boxes of  $O_{ref}$  and  $O_g$ s' contours that can be covered by them, respectively.

**Algorithm 1:** Object detection and its area determination

1. **Initialize** the indicator  $actual\_size$
2. **Initialize** input image source (  $videoSource$  )  $\leftarrow$  Endoscopic camera
3.  $f_i = videoSource.read()$
4.  $f_{i_r} = \{ Gaussian\_filter, BGR2GRAY, erode, dilate \} (f_i)$
5.  $O_A = find\_Contours( f_{i_r} )$
6. **for**  $m$  in  $O_{A_i}$  **do**:
7.     **if**  $contour\_area( O_{A_i} ) < O_{min}$  **then**:
8.         eliminate (  $O_{A_i}$  )  $\leftarrow$  update  $O_A$ 's members (  $O_{A\_updated}$  )
9.      $( O_{ref\_c}, O_{g\_c} ) = sort\_contours( O_{A\_updated} )$
10.      $( O_{ref\_c}^{np}, O_{g\_c}^{np} ) = contour\_area( O_{ref\_c}, O_{g\_c} )$
11.      $( O_{ref\_c\_box}^{np}, O_{g\_c\_box}^{np} ) = bounding\_box( O_{ref\_c}^{np}, O_{g\_c}^{np} )$
12.      $O_{ref}^{pix\_size} = \frac{O_{ref\_c\_box}^{np}}{indicator\_actual\_size}$
13.  $O_g^{actual\_size} = O_{g\_c\_box}^{np} \times O_{ref}^{pix\_size}$

In the following, the `cv2.moments` function of OpenCV is used to calculate the center of  $O_{g_c}$ , line 1, Algorithm 2. The detected contour will be cropped from the original image ( $O'_g$ ), Fig. 7d. Then  $O'_g$  will be converted to binary ( $O'_{gb}$ ). In order to invert the color of  $O'_{gb}$  we used its opposite shape, where all the white pixels inverted to black and vice versa, line 4, Algorithm 2. The contour detection process will then be used to locate new contours ( $O'_{g_c}$ ). The newly identified contours are therefore the existing gaps or holes on the  $O_g$  and the size of them will be evaluated to eliminate the undesirable ones, Fig. 7e. Moreover, the contour which has the same size as  $O_{g_c}$  will be eliminated. The center of the detected contours ( $O'_{g_{c\_updated_{x_k}}}, O'_{g_{c\_updated_{y_k}}}$ ) will be determined in x and y coordinates in the next step. Then, the size of them will be calculated, same as lines 12, 13, 14, and 16 of Algorithm 1. Finally, the distance between the newly detected contours and the original image will be calculated to determine the size of gaps by using Euclidean function from `scipy` package,  $\Delta_k$ . Note that our vision system is designed for processing one isolated item at a time.

**Algorithm 2:** Calculating the distance between the center of the object and possible gaps or holes on it.

1.  $( O_{g_{cx}}, O_{g_{cy}} ) = center( O_{g_c} )$
2.  $O'_g = crop( O_{g_c} ) \leftarrow$  cropping  $O_{g_c}$
3.  $O'_{gb} = binary( O'_g ) \leftarrow$  convert  $O_{g_c}$  to binary image
4.  $O'_{gb\_converted} = \sim O'_{gb} \leftarrow$  inverting  $O'_{gb}$  image's colour
5.  $O'_{g_c} = find\_Contours( O'_{gb\_converted} )$
6. **for**  $n$  in  $O'_{g_c}$  **do**:
7.     **if**  $contour\_area( O'_{g_{c_i}} ) < O'_{g_{c\_min}}$  **or**  $contour\_area( O'_{g_{c_i}} ) = O_{g_c}$  **then**:
8.         eliminate (  $O'_{g_{c_i}}$  )  $\leftarrow$  update  $O'_{g_c}$ 's members (  $O'_{g_{c\_updated}}$  )
9.     **for**  $k$  in  $O'_{g_{c\_updated}}$  **do**:
10.          $( O'_{g_{c\_updated_{x_k}}}, O'_{g_{c\_updated_{y_k}}} ) = center( O'_{g_{c\_updated_{k}}} )$
11.          $size\_O'_{g_{c\_updated_{k}}} =$  lines 12,13, 14, and 16 of Algorithm 1
12.          $\Delta_k = \frac{Euclidean( ( O'_{g_{c\_updated_{x_k}}}, O'_{g_{c\_updated_{y_k}}}, ( O_{g_{cx}}, O_{g_{cy}} ) )}{O_{ref}^{pix\_size}}$

**B. Autonomous Decision Making**

The major purpose of our autonomous decision-making algorithm is to select effective gripping modes, depending on the recyclable item's features, in particular size and porosity,

which will be determined using Algorithm 1 and 2. As shown in Fig. 8, the functional zones for each of the three gripping modes are  $a_h$  (claws mechanism),  $a_s$  (suction mechanism), and  $a_g$  (Nano PU mechanism). Algorithm 3 presents the autonomous decision-making process. As stated in Algorithm 3, up to three gripping modes can be activated at a time.

**Algorithm 3:** Vision based autonomous decision making.

1. **Initialize**  $adhesive = 1, vacuum\_suction = 1, paws\_claws = 1$
2. **switch** (  $O_g^{actual\_size}$  ):
3.     **case** '1': **if**  $O_g^{actual\_size}$  in range (  $a_h$  ) **then**:
4.         Func\_1(); **break**
5.     **case** '2': **if**  $O_g^{actual\_size}$  in range (  $a_s$  ) **or**  $O_g^{actual\_size} > ( a_h )$  **then**:
6.         Func\_2(); **break**
7.     **case** '3': **if**  $O_g^{actual\_size}$  in range (  $a_g$  ) **then**:
8.         active adhesive gripping module; **break**
- 9.
10. **Def** Func\_1():
11. **for**  $k$  in  $O'_{g_{c\_updated}}$  **do**:
12.     **if**  $\Delta_k = 0$  **and**  $size\_O'_{g_{c\_updated_{k}}} > a_g$  **then**:
13.          $adhesive = 0$
14.     **if**  $\Delta_k$  in range (  $a_s$  ) **then**:
15.          $t_{size\_O'_{g_{c\_updated_{k}}}} = size\_O'_{g_{c\_updated_{k}}}$
16.     **if**  $t_{size\_O'_{g_{c\_updated_{k}}}} > area( a_s )$  **then**:
17.          $vacuum\_suction = 0$
18.     **if**  $adhesive \neq 0$  **and**  $vacuum\_suction \neq 0$  **then**:
19.         active all three gripping modules.
20.     **else if**  $adhesive \neq 0$  **and**  $vacuum\_suction = 0$  **then**:
21.         active adhesive and paws\_claws gripping modules.
22.     **else**
23.         active paws\_claws gripping module.
- 24.
25. **Def** Func\_2():
26. similar to lines 11-17 Func\_1.
27. **if**  $adhesive \neq 0$  **and**  $vacuum\_suction \neq 0$  **then**:
28.     active adhesive and vacuum\_suction gripping modules.
29. **else if**  $adhesive \neq 0$  **and**  $vacuum\_suction = 0$  **then**:
30.     active adhesive gripping modules.
31. **else if**  $adhesive = 0$  **and**  $vacuum\_suction \neq 0$  **then**:
32.     active vacuum\_suction gripping modules.
33. **else**
34.     send an alarm and stop.

Based on the size of  $O_g$  and the holes on the surface of the recyclable item and the position of them relative to the center of  $O_g$ , the suitable modes for autonomous gripping onto the item is chosen. If the size of the  $O_g$  is less than the size of the  $a_h$  in mode one, three different scenarios can occur based on two conditions: condition 1 and condition 2. In the first scenario, all three gripping mechanisms will be deployed if the locations on the  $O_g$ 's surface that come to touch with the vacuum suction cups contain no holes (condition 2), and there is no hole larger than the size of the Nano PU adhesive deployable head on the  $O_g$  (condition 1), lines 18, Algorithm 3. If condition 1 is true but condition 2 is false, lines 20, Algorithm 3, the second scenario of the first gripping mode, the claws and Nano-PU adhesive mechanisms will be activated because the size of  $O_g$  is smaller than  $a_h$ . In the last

scenario of the first gripping mode, if the first and second conditions cannot be satisfied, then the only mechanism that will be activated is the claws mechanism, lines 22 and 23, Algorithm 3.

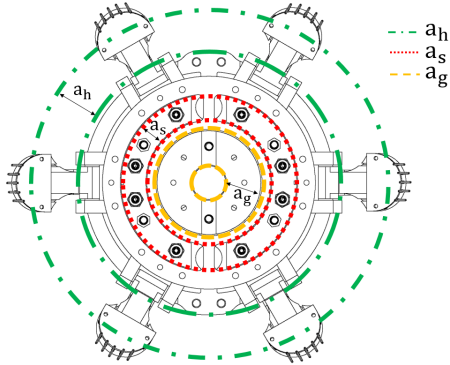


Fig. 8. Effective gripping zones when different gripping modes are deployed:  $a_h$  (claws mechanism),  $a_s$  (suction mechanism), and  $a_g$  (Nano PU mechanism).

In the second scenario, the size of  $O_g$  is greater than the  $a_h$ , resulting in the activation of the claws mechanism, line 5, Algorithm 3. The second scenario has four distinct modes. The conditions for the modes in the second scenario are the same as the first scenario. If the first and second conditions are met, the vacuum suction and Nano PU adhesive mechanisms, lines 27 and 28, Algorithm 3, will be activated. In the second mode of the second scenario, if the first condition is met but the second is not, only the Nano PU adhesive mechanism is activated. The third mode is the inverse of the second, with the vacuum suction being the only activated mechanism. When none of the gripping mechanisms can grip onto the item, the final mode of the second scenario occurs. In this case, an alarm is sent to the operator, and the system will shut down. In Algorithm 3, lines 31 and 32, when the size of  $O_g$  is within the range of  $a_g$ , the third gripping mode which is the Nano PU adhesive mechanism will be activated, lines 7 and 8.

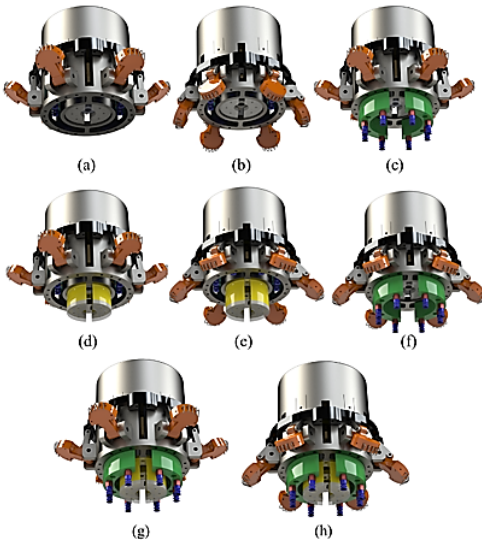
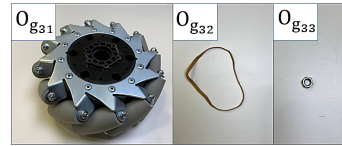


Fig. 9. Different deployment scenarios of the gripping mechanisms: (a) none of the gripping mechanisms is deployed, (b) claws are deployed, (c) vacuum suction is deployed, (d) Nano PU adhesive is deployed, (e) claws and Nano PU adhesive are deployed, (f) vacuum suction and claws are deployed, (g) vacuum suction and Nano PU adhesive are deployed, (h) all three modes are deployed.

The various opportunities for the deployment of the gripping mechanisms is shown in Fig. 9.

item number	$O_{g1}$	$O_{g2}$	$O_{g3}$	$O_{g4}$	$O_{g5}$	$O_{g6}$	$O_{g7}$
weight (kg)	1.4	0.083	0.07	0.027	0.34	0.010	0.032
size ( $l_1 \times l_2$ ) (cm)	32×25	10×10	21×21	6.8×5	24.5×16	19.5×15	16
gripping mode	$G_1 + G_2$	$G_1, G_2$	$G_1, G_2$	$G_1$	$G_1, G_2$	$G_1, G_2$	$G_1$
item number	$O_{g8}$	$O_{g9}$	$O_{g10}$	$O_{g11}$	$O_{g12}$	$O_{g13}$	$O_{g14}$
weight (kg)	0.537	0.155	0.309	0.28	0.052	0.1	1.5
size ( $d$ ) (cm)	19.5	19.5	20	19.5	9.5	19.5	19
grasping mode	$G_2, G_3$	$G_1, G_3$	$G_1, G_2, G_3$	$G_3$	$G_1, G_2$	$G_3$	$G_1, G_2, G_3$
item number	$O_{g15}$	$O_{g16}$	$O_{g17}$	$O_{g18}$	$O_{g19}$	$O_{g20}$	$O_{g21}$
weight (kg)	0.003	0.250	0.27	0.11	0.003	0.002	0.012
size ( $d_1 \times d_2 \times l$ ) (cm)	9×12×7	9×13×7	5.5×15×7	5.5×22×8	9×12×7	3.7	8
grasping mode	$G_1, G_2$	$G_1, G_2$	$G_1$	$G_1$	$G_1, G_2$	$G_1$	$G_1$
item number	$O_{g22}$	$O_{g23}$	$O_{g24}$	$O_{g25}$	$O_{g26}$	$O_{g27}$	$O_{g28}$
weight (kg)	0.12	0.08	0.045	0.195	0.082	0.006	0.011
size ( $l_1 \times l_2$ ) (cm)	12×18	11	12	19	21	2.2	4.5
grasping mode	$G_1, G_2$	$G_1$	$G_1$	$G_1$	$G_1$	$G_1$	$G_1$
item number	$O_{g29}$	$O_{g30}$	$O_{g31}$	$O_{g32}$	$O_{g33}$	$O_{g34}$	$O_{g35}$
weight (kg)	0.12	0.08	0.045	0.195	0.082	0.006	0.011
size ( $l_1 \times l_2$ ) (cm)	12×18	11	12	19	21	2.2	4.5
grasping mode	$G_1, G_2$	$G_1$	$G_1$	$G_1$	$G_1$	$G_1$	$G_1$

(a)



(b)

Fig. 10. The set of 33 laboratory recyclable items used for experimental testing: (a) graspable and releasable items, and (b) ungraspable ( $O_{g31}$ ) and unreleasable ( $O_{g32}$  and  $O_{g33}$ ) items within the set.

#### IV. EXPERIMENTAL RESULTS

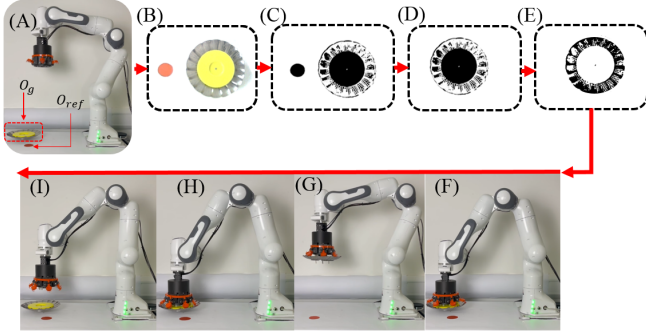
A total of 33 different recyclable items were selected for experimental testing. The items chosen for the testing are predominantly recyclable items of our robotics laboratory spanning from packaging materials to defective 3D-printed and casted parts (including hybrid-material prototypes with complex geometries) and damaged prototyping tools. Fig.10 describes the items' numbers, sizes, weights and gripping mode ( $G_1$ : Nano PU,  $G_2$ : vacuum suction, and  $G_3$ : claws). The gripping tests were performed when the recyclable items were already put in an ideal gripping posture.

As the payload of the manipulator is restricted to 3 kg, the maximum weight of the recyclable item, that should satisfy the limit, is considered as a criterion in the selection of items for experimental testing. The claws mechanism was tested non-destructively to a maximum proof load of 2.1 kg. The maximum payload that the bespoke vacuum suction and Nano PU adhesive mechanisms can hold were measured as 1.03 kg and 0.70 kg, respectively.

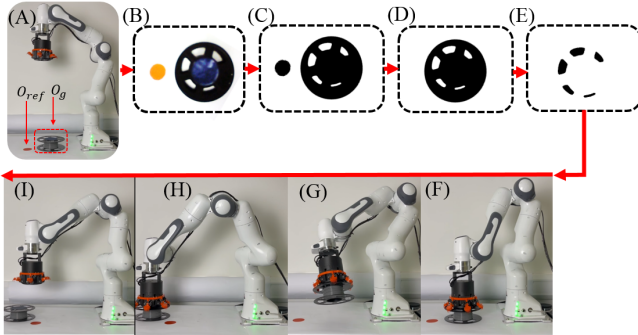
TABLE I. Gripping tests' results in different modes.

	Total items	Grasable items							Not releasable
		Nano PU adhesive	Vacuum suction	Claws	Nano PU adhesive + Vacuum suction	Nano PU adhesive + Claws	Vacuum suction + Claws	Nano PU adhesive + Vacuum suction + Claws	
<b>All objects</b>	33	28 84.84%	12 36.36%	6 18.18%	30 90.90%	29 87.87%	16 48.48%	32 96.96%	2 6.6%

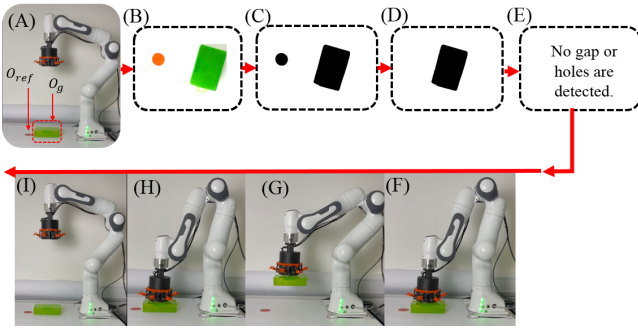
Apart from the weight, the size of the recyclable item also affects the possibility of gripping via the claws mechanism which has a minimum and maximum aperture of 12 cm and 22 cm, respectively (zone  $a_h$  in Fig. 8).



(a)



(b)



(c)

Fig. 11. The complete process of vision-based decision making, and pick and placing items using ( $O_{g10}$ , all three mechanisms), ( $O_{g9}$ , Nano PU adhesive and claws) and ( $O_{g22}$ , Nano PU adhesive and vacuum suction).

In order to use the vacuum suction and Nano PU mechanisms for gripping, the recyclable item should be contacted with the relevant mechanisms in zone  $a_s$  and zone  $a_g$ , respectively.

Three items were identified as ungraspable or unreleasable and described in Fig. 10b. Note that the lack of ability to grasp or release these items is relevant to the mechanical design of the gripping system or payload limits of the robotic manipulator rather than the decision-making algorithm. The first item is a robot wheel with a weight of 3.5 kg, which is too heavy as a payload, the second item is a rubber band that can be grasped when it is contacted with the Nano PU adhesion mechanism. However, the Nano PU releasing mechanism is not able to release it due to the flexibility and stretchability of the item. The third object is a metal nut which can be grasped if coming in touch with the Nano PU mechanism (zone  $a_g$  in Fig. 8), however it cannot be released due to the small size.

Figure 11 shows the complete pick and place process via our vision-based decision-making approach for three different recyclable items made from perforated metal and ABS plastic (Fig. 11a), plastic and silicone rubber (Fig. 11b), and plastic (Fig. 11c).

In order to evaluate the performance of our trimodal gripping module and the complimentary vision-based decision-making algorithm, a series of pick and place experiments with the set of 33 recyclable items were conducted, described in Fig. 12.

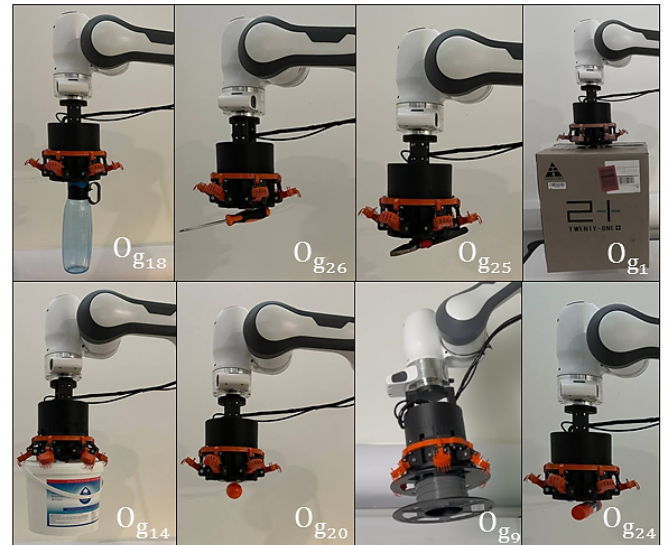


Fig. 12. Demonstration of gripping to a set of irregular items including a water bottle ( $O_{g18}$ , Nano PU), a screw driver ( $O_{g26}$ , Nano PU), a plier ( $O_{g25}$ , Nano PU), a cardboard box ( $O_{g1}$ , Nano PU + Vacuum suction), a sanitizer container ( $O_{g14}$ , Nano PU + Vacuum suction + Claws), a ping-pong ball ( $O_{g20}$ , Nano PU), a modified filament reel ( $O_{g9}$ , Nano PU + Claws), and a paper glue ( $O_{g24}$ , Nano PU).

TABLE I shows the experimental results where different gripping mechanisms were deployed individually and in combination with one another. In the first set of experiments where only one mechanism is deployed the Nano PU adhesive mechanism demonstrates the best performance enabling grasp of 84.84% of the recyclable items. In the second set of experiments two modes of gripping (out of three) were activated at a time, where the combination of Nano PU and vacuum suction shows the best performance enabling grasp of 90.90% of the recyclable items. In the third set of experiments all three gripping modes were activated at the same time enabling grasp of 96.96% of the items. As mentioned earlier, among the recyclable items, two items were not releasable due to material flexibility (a rubber band) and small size (a metal nut).

## V. CONCLUSIONS

A trimodal adaptive end-effector is developed that can be integrated with robotic sorting systems to improve their gripping versatility. Using a vision-based decision-making algorithm, the end-effector can deploy effective modes of gripping to different recyclable items in response to their surface structures, size and porosity via gripping mechanisms based on Nano Polyurethane (PU) adhesives, pumpless vacuum suction, and radially deployable claws. The results of the experiments confirmed the ability of our vision-based approach to identifying suitable gripping modes in real-time, deployment and gripping onto a wide range of our laboratory recyclable items. The experimental testing was performed on 33 laboratory recyclable items where one or more gripping modes were deployed at a time. When the modes are individually deployed using the Nano PU adhesive, vacuum suction and claws mechanism, it was possible to grasp 84.84%, 36.36%, 18.18% of the recyclable items, respectively. When two modes of gripping were activated at a time, the combination of Nano PU and vacuum suction shows the best performance enabling grasp of 90.90% of the recyclable items. By activating all three gripping modes at the same time it was possible to grasp of 96.96% of the items.

In the future work, a load cell can be integrated with the surface on which the recyclable item is placed, e.g. a conveyor belt, to measure the weight of item and communicate this information to the gripping module to optimize the decision-making process on the activation of multiple modes of gripping. Furthermore, future studies will consider improvements to the vision system so that it can deal with applications in cultured recycling environments. This will include the addition of a depth camera replacing the scaling reference sticker that may be occluded from vision in such environments.

## ACKNOWLEDGEMENT

The work is supported the EPSRC UKRI Fellowship (EP/S001840/1). Authors would like to thank industrial partners of the project 3M, Ultimaker and Behavioural Robotics Ltd.

## REFERENCES

- [1] L. Jingyi, P. Balatti, K. Ellis, D. Hadjivelichkov, D. Stoyanov, A. Ajoudani, and D. Kanoulas. "Garbage collection and sorting with a mobile manipulator using deep learning and whole-body control." *Humanoids*, 2020.
- [2] A. Zeng, S. Song, K. T. Yu, E. Donlon, F. R. Hogan, M. Bauza, D. Ma et al. "Robotic pick-and-place of novel objects in clutter with multi-affordance grasping and cross-domain image matching." In 2018 IEEE international conference on robotics and automation (ICRA), pp. 3750-3757. IEEE, 2018.
- [3] M. Schwarz, L. Christian, G. M. García, S. Koo, A. S. Periyasamy, Michael Schreiber, and Sven Behnke. "Fast object learning and dual-arm coordination for cluttered stowing, picking, and packing." In 2018 IEEE International Conference on Robotics and Automation (ICRA), pp. 3347-3354. IEEE, 2018.
- [4] D. Morrison, A. W. Tow, M. Mctaggart, R. Smith, N. K. Boxall, S. W. Mccue, J. Erskine et al. "Cartman: The low-cost cartesian manipulator that won the amazon robotics challenge." In 2018 IEEE International Conference on Robotics and Automation (ICRA), pp. 7757-7764. IEEE, 2018.
- [5] L. Chin, F. Barscevicus, J. Lipton, and D. Rus. "Multiplexed manipulation: Versatile multimodal grasping via a hybrid soft gripper." In 2020 IEEE International Conference on Robotics and Automation (ICRA), pp. 8949-8955. IEEE, 2020.
- [6] R. Sadeghian, P. Sareh, S. Shahin, S. Sareh, "Autonomous Decision Making in a Bioinspired Adaptive Robotic Anchoring Module", In 2021 IEEE/RSJ International Conference on Intelligent Robots and Systems (IROS), IEEE, 2021.
- [7] A. Parness, "Anchoring foot mechanisms for sampling and mobility in microgravity." In 2011 IEEE International Conference on Robotics and Automation, pp. 6596-6599. IEEE, 2011.
- [8] S. Shahrooz, R. Sadeghian, and S. Sareh. "Faster R-CNN-based Decision Making in a Novel Adaptive Dual-Mode Robotic Anchoring System." In 2021 IEEE International Conference on Robotics and Automation (ICRA), pp. 1-7. Royal College of Art, 2021.
- [9] H. Kaiming, G. Gkioxari, P. Dollár, and R. Girshick. "Mask r-cnn." In Proceedings of the IEEE international conference on computer vision, pp. 2961-2969. 2017.
- [10] J. Redmon, and A. Farhadi. "Yolov3: An incremental improvement." arXiv preprint arXiv:1804.02767, 2018.
- [11] L. Wei, D. Anguelov, D. Erhan, C. Szegedy, S. Reed, C. Y. Fu, and A. C. Berg. "Ssd: Single shot multibox detector." In European conference on computer vision, pp. 21-37. Springer, Cham, 2016.
- [12] S. Renato, A. Curtis, L. Kandlbauer, K. Khodier, K. E. Lorber, and R. Pomberger. "Digitalisation and intelligent robotics in value chain of circular economy oriented waste management—A review." *Waste Management* 95, 476-492, 2019.
- [13] S. Sareh, K. Althoefer, M. Li, Y. Noh, F. Tramacere, P. Sareh, B. Mazzolai, M. Kovac (2017) Anchoring like octopus: biologically inspired soft artificial sucker, *Journal of the Royal Society Interface*, 14:135.
- [14] P. B. Narayana. "Design and implementation of novel image segmentation and BLOB detection algorithm for real-time video surveillance using DaVinci processor." In 2014 International Conference on Advances in Computing, Communications and Informatics (ICACCI), pp. 1909-1915. IEEE, 2014.
- [15] R. Sadeghian, and S. Sareh. "Multifunctional arm for telerobotic wind turbine blade repair." In 2021 IEEE International Conference on Robotics and Automation (ICRA), pp. 1-7. Royal College of Art, 2021.
- [16] Himanshu. Singh, "Advanced image processing using opencv." In *Practical Machine Learning and Image Processing*, pp. 63-88. Apress, Berkeley, CA, 2019.
- [17] A. Fitwi, Y. Chen, H. Sun, and R. Harrod, "Estimating interpersonal distance and crowd density with a single-edge camera," *Computers*, vol. 10, no. 11, p. 143, Nov. 2021.